Phase Behavior and Microdomain Structure in Perfluorosulfonated Ionomers via Self-Consistent Mean Field Theory

Jeffrey J. Krueger, Philip P. Simon, and Harry J. Ploehn*

Department of Chemical Engineering, University of South Carolina, Swearingen Engineering Center, Columbia, South Carolina 29208

Received December 5, 2000; Revised Manuscript Received April 17, 2002

ABSTRACT: This paper describes the use of lattice-based self-consistent mean field (SCMF) theory to predict the equilibrium microstructure in perfluorinated ionomers used as separators in polymer electrolyte membrane (PEM) fuel cells. The SCMF model predicts segregation of ionomer−water mixtures into ionomer-rich and water-rich microdomains as the water content or the fluorocarbon−water interaction parameter (χ_{FW}) increases. Phase diagrams and domain structures are reported for water-swollen Nafion, Dow Short Side Chain, a new perfluorosulfonimide, and two other hypothetical ionomers. In general, the phase boundary for melting of the microdomain structure moves to lower values of χ_{FW} as the branch density decreases or the branch hydrophilicity increases. For ionomers having the same branch density and branch hydrophilicity, the position of the phase boundary depends on the details of the internal arrangement of chemical groups within the branches. Various phase transitions occur due to segregation of particular ionomer chemical groups and can be rationalized in terms of the dominant fluorocarbon−water repulsion and branch stretching to maximize ether−water and sulfonyl−water contacts. With increasing χ_{FW}, branch collapse minimizes the fluorocarbon−water interaction while increasing the size of water-rich domains and the degree of sulfonyl segregation.

I. Introduction

I.A. Perfluorosulfonated Ionomers. Perfluorosulfonated ionomers are branched copolymers containing comonomers that differ greatly in surface energy and electrical properties. The majority comonomer, tetrafluoroethylene (TFE), polymerizes to form hydrophobic blocks having a low dielectric constant. The minority comonomer, vinyl ether sulfonic acid, introduces hydrophilic branches that carry an ionogenic sulfonyl group. The juxtaposition within one macromolecule of comonomers with such different properties produces polymers with unique microstructures and bulk properties. For example, perfluorosulfonated ionomers swell with water and can transport ions despite the fact that the copolymer is 90% TFE. This makes these ionomers (e.g., Nafion) useful as selective transport membranes in fuel cells, chloralkali cells, and various other electrochemical synthesis/recovery cells.[1]

Membranes of perfluorosulfonated ionomers transport water and small cations (H_3O^+, Na^+, K^+) while excluding molecules as small as hydrogen gas. X-ray scattering[2] reveals the existence of ionic domains and crystallites within a continuum of amorphous polymer. The crystallites have a characteristic size that corresponds to that of PTFE crystals. The charged branch groups self-assemble to form ionic domains that swell upon exposure to water. The water-swollen ionic domains percolate so as to provide a pathway for ionic transport. Despite extensive study[3−14] of ionic transport in perfluorosulfonated ionomers, the relationship between transport properties and microstructure in these materials is poorly understood, perhaps due to a lack of consensus on the exact morphology of the phase-separated microdomains.

The composition and number density of branches have a large impact on the properties of perfluorosulfonated ionomers. Tant et al.[15] found that the dynamic mechanical and thermal properties of perfluorosulfonated ionomers varied considerably with branch density and composition. These architectural changes also have been shown to impact the impedance and conductivity of the material.[16,17] In principle, variations in molecular architecture alter the microdomain structure and thus change the material's bulk properties.

This leads to the prospect of improving the ionic transport and mechanical properties of ionomers by identifying molecular architectures that lead to optimal microdomain structures. For example, new classes of ionomers, such as those based on the sulfonimide moiety,[18] may manifest improved transport and thermomechanical properties and thus supplant Nafion in fuel cell applications. Unfortunately, such experimental exploration requires considerable investment of time and money but does not guarantee success. Theoretical models, such as the one presented here, may help guide synthesis efforts in the most fruitful directions.

I.B. Self-Consistent Mean Field Theory. This work applies self-consistent mean field (SCMF) theory to develop a thermodynamic model for predicting microstructure in perfluorosulfonated ionomers. SCMF theory provides a mathematical framework, within the context of statistical thermodynamics, for calculating the free energy of polymer/solvent mixtures in which the components are unevenly distributed in a specified spatial domain. Minimization of the free energy determines the equilibrium distribution of the components in space, represented by volume fraction $\phi_i(\mathbf{r})$ for component i at spatial position $\mathbf{r}$.

The tractability of this problem depends on a number of key approximations. In particular, the atomic-level description of real molecules must be replaced by a course-grained description that preserves the essential physical phenomena yet eliminates unnecessary details. Two main approaches have evolved within the context of SCMF theory. The continuum approach[19−22] views polymer molecules as continuous space curves with

10.1021/ma0020638 CCC: $22.00
Published on Web 05/22/2002

Polymer	Chemical Structure	Segmental Representation
Dow Short Side Chain (DSSC)	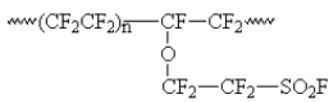	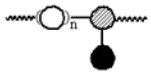
Nafion	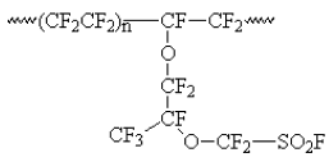	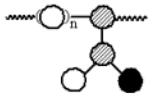
Polymer A	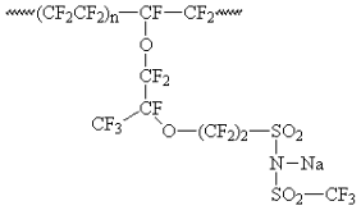	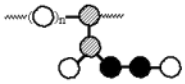
Long Dow (LD)		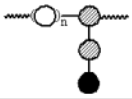
Extra Long Branch (ELB)		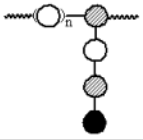

Figure 1. Molecular structures and segmental representations of various real and hypothetical ionomers.

chain stiffness and interactions represented by persistence length and excluded-volume parameters. The lattice-based approach[23] represents polymer molecules as chains of statistical segments that, along with small molecule components, fill a spatial domain discretized into lattice sites. Although the two approaches differ in details, they construct equivalent expressions for the partition function and free energy, and they minimize the free energy to identify expressions that can be solved for the equilibrium distribution of components in the spatial domain.

The application of SCMF theory for the prediction of microstructure in polymers, especially microdomain phase separation, is well established. SCMF models developed for prediction of microstructure and microdomain phase separation in linear block copolymers have been recently reviewed.[24,25] Various applications of SCMF theory involving branched block copolymers have been published.[26−28] Limited work has been done to extend SCMF theory to treat more complex architectures involving multiple block types with branching. Single-chain SCMF models[29,30] require as input an enumeration of all possible configurations of a single polymer chain. This enumeration is impractical for high molecular weight branched ionomers.

Several existing SCMF models[26,31,32] consider the problem of identifying the most favored microdomain structure. For example, Svensson et al.[31] report phase diagrams showing conditions favoring phase separation of poly(ethylene oxide)/poly(propylene oxide) triblock copolymer into various phases, including lamellae, hexagonally packed cylinders, cubic packed spheres, and bicontinuous gyroids. Such predictions are currently feasible only for macromolecules with relatively simple architecture.

Simon and Ploehn[33] developed a SCMF model that can treat branched copolymers of arbitrary architectural complexity. This model, utilized here without modification, only considers compositional variations in one Cartesian spatial dimension. For this reason, only lamellar phase-separated structures can be observed. Although the model cannot conclusively identify the preferred equilibrium geometry (e.g., lamellar, cylindrical, spheroidal, etc.), we believe that the present work is a useful first step in this direction.

I.C. Outline. First, we review SCMF theory and discuss parameter selection. The model is used to generate phase diagrams for a particular ionomer architecture (Dow Short Side Chain, DSSC) while exploring the effects of varying equivalent weight (EW, i.e., molecular weight per branch). We compare the phase diagrams of DSSC and Nafion ionomers and discuss the consequences of differing branch lengths. Finally, we explore the effect of branch *architecture* on microdomain phase separation for a variety of candidate ionomers (Figure 1), all having PTFE backbones but differing comonomers and thus differing branch architectures. The comonomers include sulfonic acid functionalities (Nafion, DSSC), a recently synthesized sulfonimide (polymer A[18]), and two "hypothetical" ionomers that have no experimental analogues. We explore the effect of branch architecture, including length, composition, and group arrangement, on the phase separation and microdomain structure.

II. Lattice-Based SCMF Theory

Lattice-based SCMF theory employs a coarse-grained representation of real polymer molecules as chains of segments. The polymers of interest in this work are

Table 1. Segment Compositions and Interaction Parameters

segment	structures		interaction parameters F	E	S	W
fluorocarbon	$-CF_2-CF_2-$, $-CF_3$	F	0	−0.5	0	varies
ether	$-CF_2-CF-O-CF_2-$, $-CF_2-O-CF-$, $-CF_2-CF-O-CF-CF_2-$	E	−0.5	0	0	−5.0
sulfonyl fluoride	SO_2F	S	0	0	0	−5.0
sulfonyl imide	SO_2NSO_2					
water	H_2O	W	varies	−5.0	−5.0	0

depicted in Figure 1. A coarse-grained representation of these molecules necessitates the introduction of three distinct segment types, fluorocarbon, ether, and sulfonyl fluoride (subscripts F, E, and S, respectively), as listed in Table 1. In addition, a segment type for the solvent, water (subscript W), is also required. Table 1 also shows various chemical structures that may be represented in the model by each segment type. All segments are assumed to have identical volumes. As shown in Figure 1, the three segment types are assembled to represent the various ionomer architectures. In addition to the three real ionomers (DSSC, Nafion, polymer A), we have also created two hypothetical ionomers, Long Dow (LD) and Extra Long Branch (ELB), to investigate the effect of architecture on phase-separated microdomain structure.

II.A. Governing Equations. Lattice-based SCMF theory offers some computational advantages for generating predictions of microstructure in branched copolymers.[34] This work utilizes the SCMF model originally developed by Evers et al.[35] and extended by Simon and Ploehn[33] to exclude direct backfolding in the calculation of chain end probability distributions. The reader may consult ref 35 for the full statistical mechanical derivation.

The primary objective is to calculate the volume fraction $\phi_A(z)$ of each segment type A (A $\in$ {F,E,S,W}) throughout the spatial domain. We consider variations in one rectangular Cartesian coordinate, z, with lattice sites arranged in layers numbered from $z = 1$ to M. Consequently, only lamellar structures are expected in the phase-separated state. The ionomer−water mixture is bounded by two impenetrable walls that have neutral interactions with all segments. Each lattice site is surrounded by y neighboring sites. A fraction λ_0 of the neighboring sites are in the same lattice layer, and a fraction λ_1 are found in each adjacent layer. All calculations reported here employed a hexagonal lattice ($y = 6$, $\lambda_0 = 1/2$, $\lambda_1 = 1/4$).

The segment volume fractions are calculated from a larger set of more detailed volume fraction profiles, $\phi_i(z,s)$, representing the volume fraction of a particular segment (rank s) belonging to a molecule of component i (i = ionomer or solvent in this work). Specifically,

$$\phi_A(z) = \sum_i \sum_{s\in\{s_A\}} \phi_i(z,s) \tag{1}$$

where the first sum runs over the components, and the second sum runs over all segments in that component with only segments of type A counted in the sum. For a linear polymer, the rank variable s is a simple enumeration of segments running from 1 to r_i, the number of segments in the chain. The segments in a branched polymer can also be numbered from 1 to r_i, obviously, but the value of s does not correspond to a distance along the contour of the polymer backbone from one of the ends.

The function $\phi_i(z,s)$ is the probability that segment number s in component i is located at position z. For any component composed of more than one segment (e.g., the ionomer), $\phi_i(z,s)$ is proportional to the joint probability that two parts of the molecule are joined by segment s at position z. To quantify this, we[33,35] first define the chain end distribution function $G_i(z,s|1)$, representing the statistical weight of all subchains (portions of whole chains) consisting of segments 1 through s that end with segment s in layer z. $G_i(z,s|1)$ is constructed recursively by multiplying G_i for a chain of s segments by the "free segment" probability, $\exp[-u_{A(s)}(z)]$, to produce G_i for a chain of $s + 1$ segments. The dimensionless mean field, $u_{A(s)}(z)$, depends on spatial position as well as the type of segment A in the molecule's structure as segment s.

For linear polymers, G_i for the entire chain can be constructed by starting with the free segment probability for either end segment, followed by multiplication of free segment probabilities going down the chain to the other end. For highly branched polymers, it is most convenient to start the product at the ends of the branches (in parallel), working backward along the branches and down the backbone to an end. The recursion for G_i thus has the form

$$G_i(z,s|r_i) = \exp[-u_{A(s)}(z)]\langle G_i(z,s+1|r_i)\rangle \tag{2}$$

with the initial value $G_i(z,r_i|r_i) \equiv 1$ since chain ends may be located anywhere with equal probability. The angle brackets in eq 2 imply a weighted average over the lattice sites neighboring the site at z:

$$\langle G_i(z,s|r_i)\rangle \equiv \lambda_1 G_i(z-1,s|r_i) + \lambda_0 G_i(z,s|r_i) + \lambda_1 G_i(z+1,s|r_i) \tag{3}$$

where λ_0 and λ_1 are the lattice parameters introduced earlier.

If we know the mean fields $u_A(z)$ for each segment type, the functions $G_i(z,s|1)$ and $G_i(z,s|r_i)$ may be readily computed. From these, $\phi_i(z,s)$ is expressed as[33,35]

$$\phi_i(z,s) = C_i \exp[-u_{A(s)}(z)]\langle G_i(z,s-1|1)\langle G_i(z,s+1|r_i)\rangle\rangle \tag{4}$$

where C_i is a normalization constant,

$$C_i = \frac{\phi_i^b}{r_i}\left(\frac{y}{y-1}\right)^{r_i-2}\left(\frac{y-1}{y-2}\right)^{b_{3i}} \tag{5}$$

Here, ϕ_i^b is the volume fraction of component i in the "bulk" reference phase, assumed to be a homogeneous mixture of the components. Also, b_{3i} is the number of three-armed branch segments in component i, and y is the lattice coordination number. Equation 4 assumes that direct backfolding is permitted. Chain branching and the exclusion of direct backfolding add considerable

complexity to the recursion expression. Reference 33 provides full, explicit details on the chain weighting factor calculation for branched polymers.

To provide closure of the set of equations, the mean fields must be specified. The statistical mechanical development[35] provides the functional forms of $u_A(z)$, ensuring an equilibrium distribution of segments as well as full occupancy of each lattice site. The free energy minimization handles the latter constraint through the introduction of a Lagrange multiplier, $\alpha(z)$. At equilibrium, $u_A(z)$, $\alpha(z)$, and $\phi_A(z)$ are related by

$$\alpha(z) = u_A(z) - \sum_i \frac{\phi_i^b}{r_i} - \frac{1}{2}\sum_{B,C}\phi_B^b \chi_{BC} \phi_C^b - \sum_B \chi_{AB} \frac{(\langle\phi_B(z)\rangle - \phi_B^b)}{\sum_C \phi_C(z)} \equiv \alpha_A(z) \quad (6)$$

The sum in the denominator of the last term should be unity, but it is included explicitly in the calculations as indicated to facilitate convergence of the iterative solution.

The right-hand side of eq 6 defines $\alpha_A(z)$. These quantities for each segment type must all equal $\alpha(z)$. The solution of the complete set of equations must satisfy this condition. The nonlinearity and complexity of the equations necessitates an iterative solution. Following the procedure found in Appendix III of the work of Evers et al.,[35] we vary $u_A(z)$ until the objective functions

$$f_A(z) = 1 - \frac{1}{\sum_A \phi_A(z)} + \bar{\alpha}(z) - \alpha_A(z) = 0 \quad (7)$$

are made equal to zero. Here $\bar{\alpha}(z)$ is the average of the $\alpha_A(z)$. For a system involving N segment types distributed over a lattice of M layers, eq 7 represents a set of NM objective functions. At any iteration, the NM guessed values of $u_A(z)$ are updated via a Newton–Raphson technique followed by recalculation of $\phi_A(z)$, $\alpha_A(z)$, and $\bar{\alpha}(z)$.

Once the equilibrium volume fraction profiles are determined, the Helmholtz free energy is calculated as given previously:[35]

$$\frac{A - A^*}{LkT} = \sum_i \frac{\ln r_i C_i}{r_i}\sum_z \phi_i(z) - \sum_{z,A}\phi_A(z)\, u_A(z) + \frac{1}{2}\sum_{z,A,B}\phi_A(z)\chi_{AB}\langle\phi_B(z)\rangle - \frac{1}{2}\sum_i[(\sum_z \phi_i(z))(\sum_{AB}\phi^*_{Ai}\chi_{AB}\phi^*_{Bi})] \quad (8)$$

The quantity ϕ^*_{Ai} represents the fraction of A-type segments in component i.

II.B. Parametrization. Very little data exist for specifying the pair interaction parameters (χ_{AB}) that quantify the interaction energy between A and B segments of the types listed in Table 1. By definition, $\chi_{AA} = 0$ for interactions between segments of the same type, leaving six independent χ_{AB} parameters to be specified. Lacking adequate data for fitting these parameters, we assume values (Table 1) that we believe approximate the true nature of the various interactions.

As seen in Table 1, ether segments represent primarily fluorinated hydrocarbon structures, yet the ether moiety introduces some polar character. Consequently, we assume that the interactions between ether and fluorocarbon segments are weakly attractive ($\chi_{FE} = -0.5$). The sulfonic acid segment is more polar, so its interactions with ether and fluorocarbon segments are less energetically favorable ($\chi_{FS} = \chi_{SE} = 0$). The attractions between water and the polar ether and sulfonic acid groups are approximated by negative values of these χ parameters ($\chi_{EW} = \chi_{SW} = -5.0$). The sulfonic acid groups will dissociate in water, but we have not incorporated electrostatic interactions in the model at this time.

Fluorocarbon and water segments will greatly outnumber the ether and sulfonyl segments in most cases. The mutual repulsion of fluorocarbon and water segments should dominate the phase behavior of the ionomer–water mixture. The corresponding pair interaction parameter, χ_{FW}, will be treated as a parameter to be varied.

All of the pair interaction parameters are temperature-dependent. For dilute polymer solutions, the Flory equation

$$\chi = \frac{1}{2} - \psi_1\left(1 - \frac{T_\theta}{T}\right) \quad (9)$$

indicates an inverse relationship between the χ and T (ψ_1 and T_θ are the entropy parameter and the theta temperature). A more complicated temperature dependence would be expected for concentrated polymer solutions and melts. Exploring temperature variations requires knowledge of $\chi_{AB}(T)$ for every AB pair. Temperature changes would simultaneously change all of the χ_{AB} values. In a sense, T parametrizes a specific path through the multidimensional χ_{AB} parameter space. Without loss of generality, we choose instead to explore independent variations of χ_{AB} values for various AB pairs. In the results reported here, we vary χ_{FW} while fixing the other χ_{AB} values. While varying χ_{FW} mimics a variation in temperature, one must bear in mind that this path through the χ_{AB} parameter space does not correspond to that path parametrized by T.

III. Results and Discussion

III.A. Phase Separation. III.A.1. General Features. We first consider the nature of the phase separation that occurs as χ_{FW} and the bulk reference phase composition (ϕ_i^b) are varied. Our SCMF theory calculations show that phase separation of ionomer–water mixtures into hydrophobic and hydrophilic domains occurs over relatively small changes in χ_{FW} or bulk phase composition. For example, Figure 2 shows volume fraction profiles for Nafion–water mixtures contained between two planar walls. At a bulk phase Nafion volume fraction of $\phi_p^b = 0.84$ (Figure 2a), the profiles of water and fluorocarbon segments are essentially flat, representing a homogeneous one-phase mixture. The depletion and small maxima near the walls are surface effects caused by the assumed absence of any ionomer–wall attraction. Not including the lattice layers immediately adjacent to the walls, the average water volume fraction is 0.16.

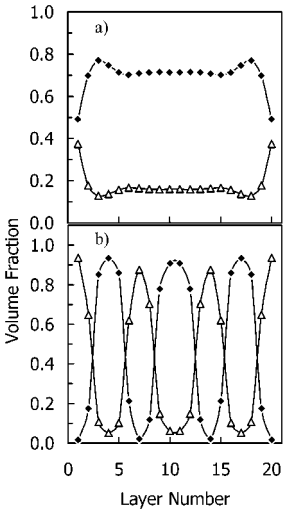

Figure 2. Volume fraction profiles of fluorocarbon (◆) and water (△) for Nafion−water mixtures with ionomer volume fractions (ϕ_i^b) of (a) 0.84 and (b) 0.82 in the bulk reference phase. Other parameters include $\chi_{FW} = 2.3$, EW = 1200, and MW = 12 000. For these parameters, n (as defined in Figure 1) = 8.

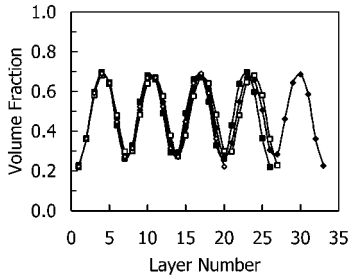

Figure 3. Fluorocarbon volume fraction profiles for DSSC−water mixtures calculated using 20 (◇), 26 (■), 27 (□), and 33 (◆) lattice layers. Other parameters include $\phi_i^b = 0.65$, $\chi_{FW} = 1.6$, EW = 1200, and MW = 12 000. For these parameters, n (as defined in Figure 1) = 9.2.

Lowering the bulk phase Nafion volume fraction to $\phi_p^b = 0.82$ (Figure 2b) leads to phase separation into fluorocarbon-rich and water-rich domains. The mixture in the domain between the surfaces is in full equilibrium with material in the bulk reference state, which is a homogeneous mixture in accord with previous work.[33,35] There is no a priori reason to expect that the average concentration in the gap between the two surfaces will be the same as in the bulk reference state. This usually presents no conceptual difficulties because, in most previous work, the bulk reference state is a stable, homogeneous, equilibrium phase. In this work, when the parameters are such that phase separation occurs, one must view the bulk reference state as a hypothetical homogeneous phase.

The observed phase separation is not an artifact of the confinement of the mixture between two planar walls, nor does the domain spacing depend on the number of lattice layers used in the calculation. Figure 3 illustrates the second point. Fluorocarbon-rich domains occur with the same spacing and amplitude regardless of the number of lattice layers used in the calculations. In this case, the domain spacing is between 6 and 7 lattice layers. As the number of layers increases, the peaks in the profiles shift to fill the space and minimize the free energy of the mixture. When the number of layers increases sufficiently, an entirely new peak appears. The free energy (eq 8) depends only on the volume fraction profiles, so the free energy density does not depend on the number of lattice layers used in the calculation. In all subsequent results shown here, the calculations employed 20 lattice layers, a compromise that provides enough space for the formation of several domains while minimizing computational time.

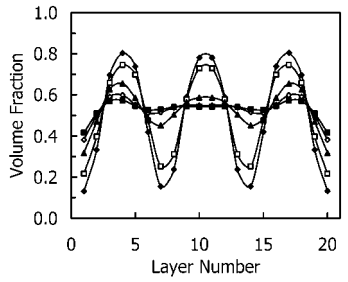

Figure 4. Fluorocarbon volume fraction profiles for Nafion−water mixtures for varying values of the fluorocarbon−water interaction parameter: $\chi_{FW} = 1.3$ (■), 1.4 (◇), 1.5 (▲), 1.6 (□), and 1.7 (◆). Other parameters include $\phi_i^b = 0.65$, EW = 1200, and MW = 12 000.

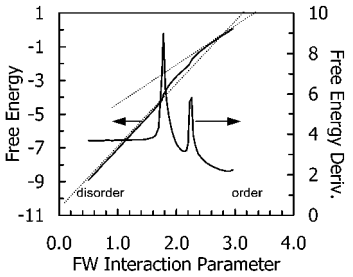

Figure 5. Helmholtz free energy and its first derivative with respect to χ_{FW} as functions of χ_{FW} for a DSSC−water mixture with $\phi_i^b = 0.65$. Other parameters include EW = 1200 and MW = 12 000. Dotted lines guide the eye with respect to the slope of the free energy before and after the transition.

In practice, it is computationally more convenient to vary χ_{FW} in order to identify points on the phase boundary. Figure 4 shows fluorocarbon volume fraction profiles for Nafion−water mixtures for various values of χ_{FW}. As χ_{FW} increases, the peaks in the fluorocarbon volume fraction profile become more pronounced, indicating greater partitioning of the hydrophobic and hydrophilic components between the two domains.

III.A.2. Free Energy Discontinuities. First-order phase transitions are characterized by discontinuities in entropy plotted as a function of temperature. This identifies phase boundaries. Regardless of the form of $\chi_{FW}(T)$, we have

$$S = -\left(\frac{\partial A}{\partial T}\right)_{V,N} \propto \left(\frac{\partial \chi_{FW}}{\partial T}\right)_{V,N}\left(\frac{\partial A}{\partial \chi_{FW}}\right)_{V,N} \qquad (10)$$

Assuming $\chi_{FW}(T)$ is continuous, $(\{\partial A\}/\{\partial \chi_{FW}\})_{V,N}$ manifests a discontinuity at a phase transition.

This derivative is calculated numerically from values of the free energy. Figure 5 shows typical results for a DSSC−water mixture having an ionomer volume fraction of 0.65 in the bulk reference phase. The free energy increases continuously as with increasing values of χ_{FW}. However, $(\{\partial A\}/\{\partial \chi_{FW}\})_{V,N}$ is discontinuous at two points, $\chi_{FW} = 1.78$ and 2.25, suggesting two phase transitions. Actually, a third discontinuity occurs at about $\chi_{FW} = 3.0$, although it cannot be seen in the figure. The initial phase separation of the mixture into fluorocarbon-rich

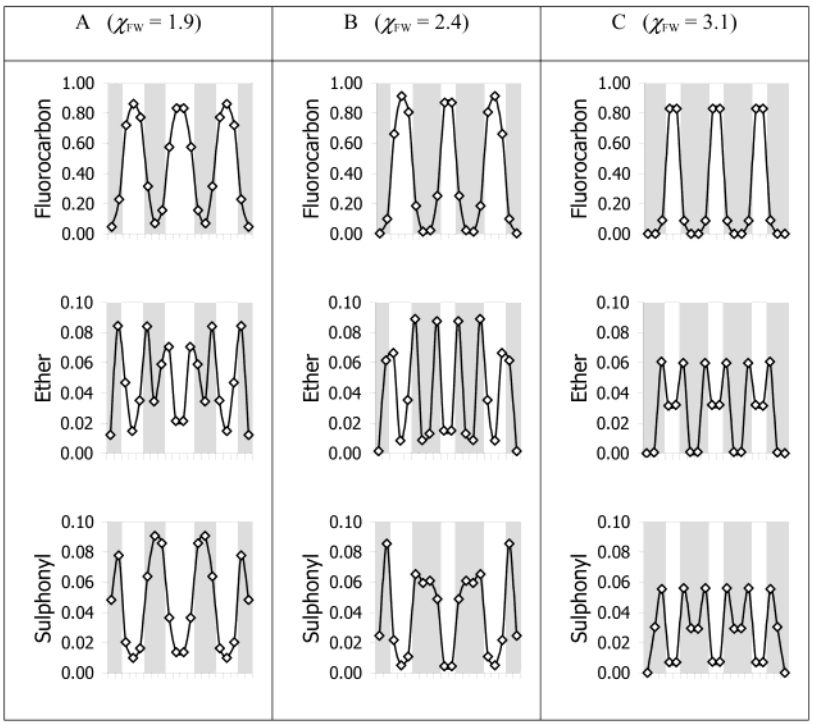

Figure 6. Volume fraction profiles of fluorocarbon, ether, and sulfonyl segments for DSSC ionomer with $\phi_i^b = 0.65$. The shaded regions denote lattice layers where the water volume fraction exceeds 50%. Columns A, B, and C are for $\chi_{FW} = 1.9$, 2.4, and 3.1, respectively, representing values that are 0.1 units higher than the preceding phase transition. Other parameters as in Figure 2 and Table 1.

and water-rich domains occurs at $\chi_{FW} = 1.78$, in agreement with qualitative observation of the appearance of peaks in the volume fraction profiles (similar to those seen in Figure 4, but for DSSC).

There are three difficulties in reconciling the observations in Figure 5 with established phase transition concepts. First, segregation occurs in several overlapping stages because of the different properties of the ionomer's constituent segments (discussed below). This produces two or more closely spaced discontinuities in the free energy, so the putative phase transitions are not very clean. Second, some inaccuracy is introduced because we are calculating the free energy derivative numerically. Finally, correspondence with thermodynamic definitions of phase transitions is hindered because we are not varying temperature, but a surrogate, χ_{FW}.

Nevertheless, the features in Figure 5 suggest that we see what may be legitimately called phase transitions. Discontinuities in free energy are characteristic of first-order phase transitions. As we increase χ_{FW}, free energy increases because the dominant fluorocarbon−water interactions become more repulsive. After the transition, the free energy continues to grow but at a lower rate (change in slope of dotted lines in Figure 5). Moving along the ordinate from right to left (or viewing a mirror image of the figure) simulates an increasing temperature axis, and the dotted lines trace out the expected form of a first-order phase transition.

Volume fraction profiles provide additional insight into the nature of the phase transitions such as those seen in Figure 5. For example, the free energy of water-swollen DSSC ionomer with $\phi_p^b = 0.75$ manifests discontinuities at χ_{FW} values of 1.85, 2.50, and 2.70, identifying three phase transitions in the system. At χ_{FW} values below 1.85, the volume fraction profiles of all segment types are essentially flat. For χ_{FW} values greater than 1.85, we observe segregation into water-rich (hydrophilic) and water-poor (hydrophobic) domains. Figure 6 shows volume fraction profiles for fluorocarbon, ether, and sulfonyl segments at χ_{FW} values that are 0.1 units greater than the phase transition points. This offset ensures that the selected states are away from the phase boundaries and that the structures are fully developed. The shaded regions represent domains where the water volume fraction exceeds 50%. All of the pair interaction parameters other than χ_{FW} have been held constant.

The predominant feature of the first phase transition is segregation of fluorocarbon and water segments into fluorocarbon-rich and water-rich domains (Figure 6A). Although the fluorocarbon domains contain most of the fluorocarbon segments, the water-rich domains also contain significant amounts of fluorocarbon (>10 vol %). Ether and sulfonyl segments are concentrated primarily in the water-rich domains. Further increase in χ_{FW} leads to a second transition characterized by elimination of the remaining fluorocarbon from the water-rich domains and localization of ether segments at the domain interfaces (Figure 6B). The water-rich domains are thicker with sulfonyl segments dispersed evenly throughout. Still further increase in χ_{FW} produces a final phase transition, above which the sulfonyl segments are more localized at the domain interfaces (Figure 6C). The water-rich domains have grown even thicker and still contain significant amounts of ether and sulfonyl segments. The fluorocarbon domains have become quite thin and somewhat enriched with ether and sulfonyl segments.

A simple physical picture explains these observations. As the interaction energy (χ_{FW}) between the dominant components—fluorocarbon and water—becomes more

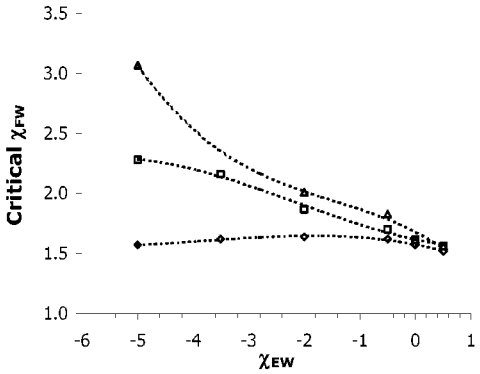

Figure 7. Critical values of χ_{FW} associated with the first (diamonds), second (squares), and third (triangles) phase transitions as functions of the ether−water interaction parameter, χ_{EW}, for DSSC ionomer with $\phi_i^b = 0.65$. Other parameters as in Figure 6.

repulsive, the system minimizes its free energy by segregating water and fluorocarbon into hydrophilic and hydrophobic domains. However, the segregation is not complete. Attractive ether−water and sulfonyl−water interactions ($\chi_{EW} = -5$, $\chi_{SW} = -5$) promote extension of the branches to maximize these contacts (Figure 6A), suggesting a picture of the water-rich domains as water-swollen polymer gels rather than "pools" of water. Many fluorocarbon−water contacts also remain. As χ_{FW} increases further, the remaining fluorocarbon−water contacts are replaced by fluorocarbon−ether and fluorocarbon−sulfonyl contacts. This happens through more complete fluorocarbon−water segregation and interposition of the ethers at the domain interface (Figure 6B). Although this requires collapse of the extended branches, the free energy reduction due to minimized fluorocarbon−water contacts dominates at large χ_{FW}. Above the third transition (Figure 6C), complete branch collapse occurs, localizing sulfonyl segments at the interface and further minimizing fluorocarbon−water contact.

III.A.3. Varying Interaction Parameters. Similar phase transitions have been found[36] for all of the candidate ionomers shown in Figure 1. The locations of the phase boundaries in the temperature−composition phase diagram obviously depend on the values of the interaction parameters as well as the ionomer architecture. Since fluorocarbon and water are the two most prevalent components, their interaction parameter (χ_{FW}) should play a dominant role. In a sense, χ_{FW} serves as a surrogate for (inverse) temperature. Variations in the other interaction parameters influence the values of χ_{FW} at which phase transitions occur, denoted below as χ_{FW}*.

As an example, consider the ether−water interaction parameter, χ_{EW}. The base value, $\chi_{EW} = -5$, assumes that polar ether oxygens manifest a strong attractive interaction with water. However, recent ab initio self-consistent-field molecular orbital calculations[37] suggest that fluoroether segments may be more hydrophobic than sulfonyl (base value $\chi_{SW} = -5$). We should therefore consider the effect of varying values of χ_{EW} on the location of phase transitions represented by χ_{FW}*. As seen in Figure 7, making the ether−water interaction less attractive has little effect on the χ_{FW}* for the first phase transition. Since fluorocarbon−water segregation drives the first phase transition, we would not expect a strong dependence on the interaction of the minor ether component with water. On the other hand, the second and third phase transitions move to lower values of χ_{FW} and eventually merge with the first phase transition as χ_{EW} increases.

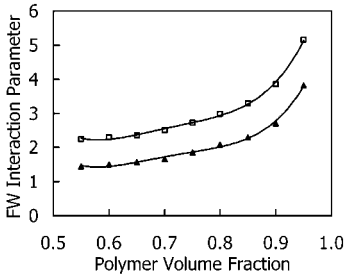

Figure 8. Phase diagrams for DSSC−water mixtures for ionomers with equivalent weights of 800 (□) and 1200 (▲). In both cases, MW = 12 000.

Physically, more positive values of χ_{EW} reduce the free energy benefit associated ether−water mixing. The branches remain stretched after the first transition, but branch collapse and ether−water demixing can occur at lower χ_{FW} values, so χ_{FW}* for the second transition decreases with increasing χ_{EW}. Eventually, for $\chi_{EW} > 0$, ether segments segregate with the fluorocarbon and sulfonyl segments localize at the interface at the first phase transition.

Similar trends have been observed for variations of the other pair interaction parameters.[36] In general, the χ_{FW}* values for the first transition (fluorocarbon−water segregation) are essentially independent of the values of other interaction parameters. The χ_{FW}* values for the second and third transitions generally decrease, approaching those for the first transition, as the value of the varied parameter increases, all others held constant. Various enthalpic and entropic factors probably explain these trends, including the amount of initial branch stretching above the first transition, the balance among the various pair interaction energies, and the entropy associated with changing the distribution of water between the domains.

III.B. Phase Diagrams. In this work, we construct theoretical phase diagrams that employ χ_{FW} and polymer (ionomer) volume fraction in the bulk reference phase (ϕ_p^b) as two parameter space coordinates. Free energy discontinuities, determined numerically, determine the locus of (ϕ_p^b, χ_{FW}) points that delineate the order−disorder phase transition.

III.B.1. General Features. Figure 8 shows the DSSC−water phase diagram for ionomers having two different branch densities. For a particular polymer, spatially homogeneous (disordered) mixtures are observed at (ϕ_p^b, χ_{FW}) points below the phase boundary, while phase-separated (ordered) states are found above the boundary. Assuming χ_{FW} varies inversely with T, increasing χ_{FW} corresponds (approximately) to a temperature quench. As expected, increasing χ_{FW} at fixed composition leads to phase separation. At fixed χ_{FW}, increasing the water content in the bulk reference phase (decreasing ϕ_p^b) leads to phase separation. A compromise between entropic and enthalpic effects explains these (and subsequent) observations. Repulsive enthalpic interactions between fluorocarbon and water segments make the free energy more positive. Ionomer−water mixing and branch stretching produce greater configurational entropy and thus reduce the free energy. Phase separation occurs when the reduction of unfavorable fluorocarbon−water interactions outweighs the loss of configurational entropy due to segregation. With

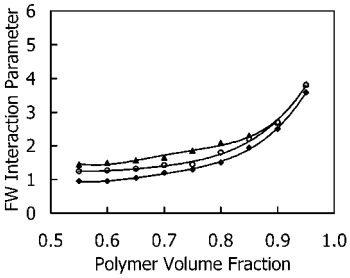

Figure 9. Phase diagrams for various ionomer−water mixtures, including DSSC (▲, EW = 1200), Nafion (○, EW = 1396), and LD (◆, EW = 1326). In all cases, MW = 12 000.

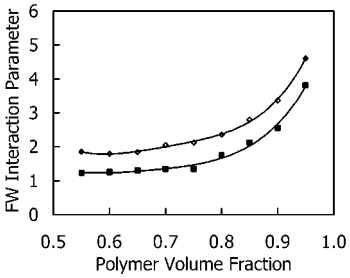

Figure 10. Phase diagrams for Nafion−water (△) and ELB−water (■) mixtures for ionomers with EW = 1200 and MW = 12 000.

decreasing water content, the critical value of χ_{FW} for phase separation increases. With fewer numbers of fluorocarbon−water contacts, the repulsion per water segment must be larger to induce segregation.

III.B.2. Branch Density. The branch density has a significant effect upon the location of the phase boundary (Figure 8). For the DSSC ionomer, increasing the equivalent weight from 800 to 1200 g/mol (or decreasing the branch density) produces a significant shift of the phase boundary to smaller values of χ_{FW}. The configurational entropy of the branches plays a role here. An ionomer with a lower branch density loses less entropy upon segregation. Because of the lower entropy penalty, phase separation is favored at a lower level of fluorocarbon−water repulsion.

In qualitative terms (treating χ_{FW} as inversely proportional to T), higher branch density shifts the phase boundary to lower temperature. Tant et al.[15] report similar trends for the glass transition temperature (T_g) and crystallinity of DSSC ionomers: for higher branch density, T_g as well as degree of crystallinity decreases. They argue that higher branch density increases steric (entropic) constraints that hinder crystallite formation and chain packing in amorphous regions, thus lowering the T_g.

III.B.3. Branch Length. Tant et al.[15] also investigated the effect of side chain (i.e., branch) length by comparing dynamic mechanical spectra and X-ray scattering results for DSSC and Nafion ionomers having the same branch density. They find that the T_g and crystallinity of the DSSC ionomer were greater than those of Nafion. They rationalize these observations by arguing that the DSSC's shorter side chains introduce less steric hindrance to amorphous packing and crystallite formation relative to the longer side chains in Nafion. However, consideration of branch length alone may be an oversimplification. Adding a segment to a branch changes not only its length but also its hydrophilicity vis-à-vis the fluorocarbon backbone.

Figure 9 shows the phase boundary in (ϕ_p^b, χ_{FW}) space for DSSC (▲) and Nafion (○) ionomers having the same branch density. The Nafion phase boundary lies below that of DSSC (i.e., at lower χ_{FW} values) for moderate water contents. The longer branches in Nafion have greater configurational entropy than those in DSSC. Thus, the entropy penalty associated with phase separation should be greater for Nafion. If the entropic effect dominates, the Nafion phase boundary ought to lie at higher χ_{FW} values than that of DSSC.

On the other hand, Nafion branches are more hydrophilic than DSSC branches. To quantify this, we define the "branch hydrophilicity" χ_{BW} as the sum of χ_{iW} over all segments in the side chain[38] ($\chi_{BW} = -13$ for Nafion and −10 for DSSC). Phase separation creates water-rich domains that permit greater contact between hydrophilic branches and water. The magnitude of fluorocarbon−water repulsion (χ_{FW}) needed to induce phase separation should decrease with increasing branch hydrophilicity (more negative values of χ_{BW}). This may explain why the Nafion phase boundary lies at lower χ_{FW} values than that of DSSC (Figure 7).

To further test this hypothesis, we performed calculations for a hypothetical ionomer, Long Dow (LD), that has an extra ether segment in each branch ($\chi_{BW} = -15$). For the same branch density, the phase boundary for LD−water mixtures (Figure 7) lies at lower χ_{FW} values than that of Nafion. If entropy effects were dominant, the LD phase boundary would lie above that of DSSC. This illustrates the point that the hydrophilicity of the branch plays a critical role in determining the conditions for microdomain phase separation.

Nevertheless, branch length—or, more generally, topology (the internal arrangement of segments)—must also influence phase behavior. The relative positions of the Nafion, DSSC, and LD phase boundaries in Figure 9 seem to be controlled branch hydrophilicity, with branch topology being a secondary factor. To explore the effect of branch topology, we have performed calculations for another hypothetical ionomer, Extra Long Branch (ELB). ELB has branches with the same hydrophilicity as those in Nafion ($\chi_{BW} = -13$) but with differing segment topology. Figure 10 compares the ELB and Nafion phase boundaries in (ϕ_p^b, χ_{FW}) space at the same branch density. The ELB phase boundary lies significantly below that of Nafion. Since χ_{BW} is the same for both ionomers, some combination of entropic and enthalpic effects arising from the branch topology must be responsible for the difference. Further rationalization based on presumptions of the relative entropy losses associated with segregation and branch stretching may be possible but would be highly speculative.

III.C. Domain Size and Composition. The transport properties of an ionomer depend on the size, shape, composition, and connectivity of the water-rich microdomains in the phase-separated state. Although the present model cannot address the shape and connectivity aspects, it can give a qualitative indication of size and composition trends. Even this limited information may useful in guiding the development of new molecular architectures.

III.C.1. Water-Rich Domain Size. First, we examine the size of the water-rich domains, defined for convenience as any contiguous set of lattice layers containing more than 50 vol % water. Figure 11 shows the size of the water-rich domains as a function of χ_{FW} for each of the candidate ionomers represented in Figure 1. For all architectures, the water-rich domain size increases with χ_{FW}. Nafion and DSSC are similar in that

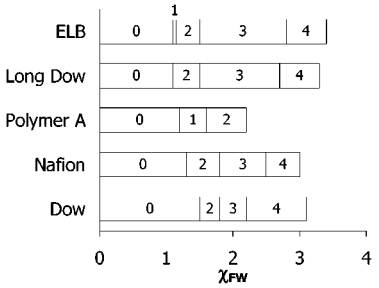

Figure 11. Size of water-rich domains (number of lattice layers as indicated in bars) as a function of χ_{FW} for ionomers having the same branch density. In all cases $\phi_i^b = 0.65$, MW = 12 000 g/mol, and have equivalents weights corresponding to nine backbone segments between branches (DSSC 1200 g/mol, Nafion 1396 g/mol, polymer A 1626 g/mol, Long Dow 1326 g/mol, and ELB 1396 g/mol). Other parameters as in Table 1.

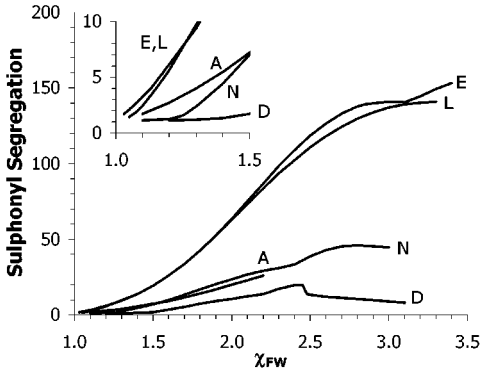

Figure 12. Variation of sulfonyl segregation factor with χ_{FW} for various ionomers swollen with 35 vol % water. The inset shows an expanded scale for low values of χ_{FW}. All other parameters as in Figure 11.

the appearance of water-rich domains occurs at relatively high χ_{FW} values. Polymer A, Long Dow, and ELB all exhibit transitions to water-rich domains at lower χ_{FW} values. The domains in polymer A remain small, while those in LD and ELB remain relatively large over a wide range of χ_{FW}. Considering χ_{FW} as a surrogate for temperature (assuming $\chi_{FW} \propto 1/T$), these observations suggest that LD and ELB might manifest water-rich domains over a wider temperature range and down to lower temperatures than any of the "real" ionomers (Nafion, DSSC, polymer A).

Despite its smaller water-rich domain size, polymer A should not be discounted as a viable candidate structure. The domain spacing in polymer A repeats every five lattice layers, while all others repeat every seven layers. Near $\chi_{FW} = 2.0$, water-rich domains occupy 40% ($^2/_5$) of the space in polymer A and 42% in the other ionomers ($^3/_7$). Thus, the proportion of the space occupies by water-rich domains is comparable for all of the candidate architectures.

III.C.2. Sulfonyl Segregation. The ionic conductivity of an ionomer presumably depends on the extent to which its ionogenic groups are available for hydration and interaction with mobile ions. For the perfluorinated ionomers considered here, we are particularly interested in partitioning of the sulfonyl groups. Under most conditions, sulfonyl groups preferentially segregate into the water-rich domains. We define a segregation factor equal to the ratio of maximum to minimum volume fractions of sulfonyl groups within one repeating domain (excluding wall regions). Figure 12 shows the sulfonyl segregation factor for all candidate ionomers as a function of χ_{FW}. Under all conditions, LD and ELB show the strongest segregation of sulfonyl groups, Nafion and polymer A show similar lower levels of sulfonyl segregation, and DSSC has the lowest segregation factor.

These results can, for the most part, be rationalized in terms of the branch architecture (Figure 1). LD and ELB both feature sulfonyl groups at the end of relatively long, linear, hydrophilic branches, thus enabling good spatial separation of sulfonyl and fluorocarbon segments. On the other hand, only one ether segment separates the branch sulfonyl from backbone fluorocarbons in the DSSC ionomer. Nafion and polymer A have intermediate levels of sulfonyl segregation for two reasons: the branches are relatively bulky, and sulfonyls are either adjacent to fluorocarbons (polymer A) or separated by one ether segment (Nafion and polymer A). The similar level of sulfonyl segregation in Nafion and polymer A is consistent with experimental observations of their similar ionic conductivities.[39] Despite the fact that Nafion and ELB have identical branch compositions, their levels of sulfonyl segregation differ greatly. This shows the sensitivity of the microdomain structure to small variations in branch architecture.

IV. Conclusions

To our knowledge, this work represents the first application of SCMF theory to describe microstructure in ionomers such as Nafion. The model introduces a number of simplifications, including a coarse-grained description of real molecules in terms of statistical segments, mean-field treatment of interactions, and restriction of phase-separated morphology to lamellar geometry. Our assumed interaction parameters are reasonable but arbitrary. Furthermore, the model does not provide a satisfactory description of the crystallinity of the fluorocarbon domains or electrostatic interactions among ionogenic groups. Despite these drawbacks, the model does provide interesting physical insights that are in qualitative agreement with experiments.

Most significantly, lattice-based SCMF theory predicts that the free energy density of water-swollen perfluorinated ionomers manifests a series of discontinuities, interpreted as phase transitions, as the value of the fluorocarbon−water interaction parameter increases. Each phase transition is accompanied by a microstructural rearrangement that reflects a compromise of enthalpic and entropic contributions to the mixture free energy. Phase diagrams can be constructed which show conditions (fluorocarbon−water interaction parameter, ionomer volume fraction in the bulk reference phase) leading to phase separation.

Although we do not explore explicit variations in temperature, χ_{FW} may serve as a surrogate, since fluorocarbon and water are the two predominant constituents. In general, we may assume that χ_{FW} decreases as temperature increases. Consequently, we can discuss in qualitative terms the implications of our results for the design of ionomers for PEM fuel cell applications. To transport ions, an ionomer membrane probably must have a phase-separated morphology with percolation of the hydrophilic domains, particularly at higher temperatures and lower water contents. In the context of the phase diagrams shown here, we would like to identify ionomers having phase boundaries that pass as close as possible to the lower right corner of the (ϕ_p^b, χ_{FW}) space.

The branch density predictions (Figure 8) suggest that, for a selected ionomer chemistry, decreasing the ionomer branch density lowers the phase boundary, in effect pushing the melting of the phase-separated microdomain structure to a higher temperature. On the other hand, decreasing the branch density would reduce the density of ionogenic sulfonyl groups, presumably leading to lower ionic conductivity. Thus, an optimum branch density should exist. At constant branch density, more hydrophilic branches promote phase separation at lower χ_{FW} values, corresponding approximately to higher temperatures (Figure 9). The internal arrangement of segments in the branch (i.e., topology) also plays an important role (Figure 10).

With respect to the water-rich domain size and the segregation of sulfonyl segments, the model results suggest that ionomers with longer branches promote the formation of larger water-rich domains with greater sulfonyl segregation. Fluorocarbon segments in the branch tend to impede water-rich domain formation and sulfonyl segregation. The sulfonimide ionomer, polymer A, may be an exception: the model suggests it may form greater numbers of smaller domains with high levels of sulfonyl segregation. The two hypothetical ionomers, Long Dow and ELB, exhibit very strong segregation of the sulfonyl segments due to the linear structure and hydrophilic nature of their branches.

If the predicted phase transitions are real, the qualitative trends may have important implications for the design and use of ionomers as membranes in fuel cells. In particular, not only should a candidate ionomer exhibit phase separation into microdomains at the operating temperature, but its architecture should also promote the formation of the most favorable structures for maximizing performance. The model presented here may yield some useful insights for guiding the efforts of synthetic chemists in the development of new ionomers for use as ion transport membranes.

Acknowledgment. We gratefully acknowledge the financial support of this research by the U.S. Department of Energy through Cooperative Agreement DE-FG02-91ER75666 and by the U.S. Army Research Laboratory and the U.S. Army Research Office under Grant DAAH04-96-1-0422.

References and Notes

(1) Risen, W. M., Jr. Applications of Ionomers. In *Ionomers: Characterization, Theory, and Applications*; Schlick, S., Ed.; CRC Press: Boca Raton, FL, 1996; p 281.
(2) Gebel, G.; Loppinet, B. Small-Angle Scattering Study of Perfluorosulfonated Ionomer Membranes and Solutions. In *Ionomers: Characterization, Theory, and Applications*; Schlick, S., Ed.; CRC Press: Boca Raton, FL, 1996; p 83.
(3) Din, X. D.; Michaelides, E. E. *AIChE J.* **1998**, *44*, 35.
(4) Bath, B. D.; White, H. S.; Scott, E. R. *Anal. Chem.* **2000**, *72*, 433.
(5) Cirkel, P. A.; Okada, T. *Macromolecules* **2000**, *33*, 4921.
(6) Danielsson, L. G.; Yang, X. T. *Anal. Chem.* **2000**, *72*, 1564.
(7) Van der Stegen, J. H. G.; van der Veen, A. J.; Weerdenburg, H.; Hogendoorn, J. A.; Versteeg, G. F. *Chem. Eng. Sci.* **1999**, *54*, 2501.
(8) Wintersgill, M. C.; Fontella, J. J. *Electrochim. Acta* **1998**, *43*, 1533.
(9) Lteif, R.; Dammak, L.; Larchet, C.; Auclair, B. *Eur. Polym. J.* **1999**, *35*, 1187.
(10) Kreuer, K. D.; Ise, M.; Fuchs, A.; Maier, J. *J. Phys. IV* **2000**, *10*, 279.
(11) Eikerling, M.; Kornyshev, A. A.; Stimming, U. *J. Phys. Chem. B* **1997**, *101*, 10807.
(12) Lehmani, A.; Bernard, O.; Turq, P. *J. Stat. Phys.* **1997**, *89*, 379.
(13) Paddison, S. J.; Paul, R.; Zawodzinski, T. A. *J. Electrochem. Soc.* **2000**, *147*, 617.
(14) Hamersky, M. W.; Tirrell, M.; Lodge, T. P. *Langmuir* **1998**, *14*, 6974.
(15) Tant, M. R.; Darst, K. P.; Lee, K. D.; Martin, C. W. Structure and Properties of Short-Side-Chain Perfluorsulfonate Ionomers. In *Multiphase Polymers: Blends and Ionomers*; Utaracki, L. A., Weiss, R. A., Eds.; *ACS Symp. Ser.* **1989**, *395*, 370.
(16) Fontella, J. J.; Edmondson, C. A.; Wintersgill, M. C.; Wu, Y.; Greenbaum, S. G. *Macromolecules* **1996**, *29*, 4944.
(17) Zaluski, C. S.; Xu, G. *J. Electrochem. Soc.* **1994**, *141*, 448.
(18) DesMarteau, D. D.; Ma, J.-J.; Liu, M.-T.; Thomas, B.; McClellan, J. *Polym. Mater. Sci. Eng.* **1999**, *80*, 598.
(19) Edwards, S. F. *Proc. Phys. Soc. London* **1965**, *85*, 613.
(20) Freed, K. F. *Adv. Chem. Phys.* **1972**, *22*, 1.
(21) De Gennes, P. G. *Rep. Prog. Phys.* **1969**, *32*, 187.
(22) Helfand, E. *J. Chem. Phys.* **1975**, *62*, 999.
(23) Scheutjens, J. M. H. M.; Fleer, G. J. *J. Phys. Chem.* **1979**, *83*, 1619. *J. Phys. Chem.* **1980**, *84*, 178. *Macromolecules* **1985**, *18*, 1882.
(24) Matsen, M. W.; Schick, M. *Curr. Opin. Colloid Interface Sci.* **1996**, *1*, 329.
(25) Bates, F. S.; Fredrickson, G. H. *Phys. Today* **1999**, *52*, 32.
(26) Drolet, F.; Fredrickson, G. H. *Phys. Rev. E* **1999**, *83*, 4317.
(27) van Lent, B.; Scheutjens, J. M. H. M. *J. Phys. Chem.* **1990**, *94*, 5033.
(28) Boris, D.; Rubinstein, M. *Macromolecules* **1996**, *29*, 7251.
(29) Muller, M.; Shick, M. *Phys. Rev. E* **1998**, *57*, 6973.
(30) Carignano, M. A.; Szleifer, I. *Europhys. Lett.* **1995**, *30*, 525.
(31) Svensson, M.; Alexandris, P.; Linse, P. *Macromolecules* **1999**, *32*, 637.
(32) Mai, S.-M.; Faircloth, J. P. A.; Hamley, I. W.; Matsen, M. W.; Denny, R. C.; Liao, B.-X.; Booth, C.; Ryan, A. J. *Macromolecules* **1996**, *29*, 6212.
(33) Simon, P. P.; Ploehn, H. J. *Macromolecules* **1998**, *31*, 5880.
(34) Janssen, R. H. C.; Nies, E.; Cifra, P. *Langmuir* **1997**, *13*, 2784.
(35) Evers, O. A.; Scheutjens, J. H. M.; Fleer, G. J. *Macromolecules* **1990**, *23*, 5221.
(36) Krueger, J. Modeling Microstructural Phase Behavior in Perfluorosulphonated Ionomers. Ph.D. Dissertation, University of South Carolina, 2000.
(37) Paddison, S. J.; Zawodzinski, T. A. *Solid State Ionics* **1998**, *115*, 333.
(38) The value of χ_{BW} equals the sum of χ_{iW} for all segments in the side chain (Table 1). Since χ_{FW} varies, we assume $\chi_{FW} = 2.0$ as an average value.
(39) Sumner, J. J.; Creager, S. E.; Ma, J. J.; DesMarteau, D. D. *J. Electrochem. Soc.* **1998**, *145*, 107.

MA0020638